Sigma J Eng Nat Sci, Vol. 44, No. 2, pp. 1172–1186, April, 2026

Sigma Journal of Engineering and Natural Sciences
Web page info: https://sigma.yildiz.edu.tr
DOI: 10.14744/sigma.2025.00141

Research Article

Investigation of correlation between standard penetration test blow counts and internal friction angles for loess soils

Murat GÜLEN[1,*]

[1]*Department of Civil Engineering, Siirt University, Siirt, 56100, Türkiye*

ARTICLE INFO

Article history
Received: 04 March 2025
Revised: 05 May 2025
Accepted: 22 July 2025

Keywords:
Direct Shear Box Test; Internal Friction Angle; Loess Soils; SPT Blow Count

ABSTRACT

The internal friction angle of soils is determined through laboratory tests. This parameter can also be estimated with high accuracy by referencing field test results. This approach enables the required soil parameters for design purposes to be determined with greater ease and reduces reliance on individual interpretation. A variety of engineering structures are constructed on rich loess deposits, and these loess soils differ significantly from other soil types. In contrast to the extensive research conducted on the strength properties of other soils, the field-test-based research on estimating the strength properties of loess soils remains quite limited. This study aims to address the gap in the literature on loess soils and contribute to this area of research. For this, standard penetration tests were conducted on Central Asian loess soils, known to be among the world's richest loess deposits. This study examined 86 samples exhibiting particle size distributions characteristic of loess soils. The samples were reconstituted in the laboratory to match their natural field water content and density, then subjected to direct shear box tests. Based on the resulting data, a correlation was proposed between standard penetration test blow counts and internal friction angles. The correlation coefficient R^2 = 0.732 indicates a moderately strong relationship. In addition, new equations were developed based on original data derived from loess soils and presented. These were then compared with the empirical relationships previously proposed for sandy soils, and the similarities and differences were interpreted in detail. These results provide practical guidance for estimating the internal friction angle of loess soils, particularly in the early stages of design when field and laboratory data may be limited.

Cite this article as: Gülen M. Investigation of correlation between standard penetration test blow counts and internal friction angles for loess soils. Sigma J Eng Nat Sci 2026;44(2):1172–1186.

INTRODUCTION

Loess soils have unique geotechnical properties that distinguish them from other soil types. Formed by wind-driven deposition, they have a loose, porous and metastable structure with variable grain sizes [1,2]. Their collapsibility under wetting and loading can lead to sudden settlement [3]. While partial cementation provides dry strength, saturation causes instability [4,5]. Its high void ratio, anisotropy

*Corresponding author.
*E-mail address: murat.gulen@siirt.edu.tr

This paper was recommended for publication in revised form by Editor-in-Chief Ahmet Selim Dalkilic

Published by Yıldız Technical University Press, İstanbul, Turkey
© Author. This is an open access article under the CC BY-NC license (http://creativecommons.org/licenses/by-nc/4.0/).

and perturbation sensitivity reduce the reliability of standard empirical models [6]. The index and engineering properties of loess soils characterised by high bearing capacity in their dry state, high porosity, low water retention potential, and sudden settlement under saturated loading have been extensively investigated by various researchers [6-8]. Firstly, there is a clear divergence of opinion among researchers regarding the definition of loess soils. Sharifi Teshnizi et al. [4] characterised loess soils as loose to medium-dense silty soils that are partially cemented by clay particles and salts. Terzaghi et al. [9] and Liu [10] describe loess soils as wind-transported deposits of sedimentary origin. Meanwhile, Assadi-Langroudi et al. [5] define them as silt particles that have formed through the direct or indirect combination of silts, clays, and carbonates. Additionally, some researchers have classified loess soils based on their grain size distribution [11–14]. In particular, Swineford and Frye [11] defined loess soils as soils containing a mixture of fine sand and coarse silt, averaging between 0.02 and 0.05 mm in size. In their respective studies, Nouaouria et al. [8] and Li et al. [15] indicated that the predominant grain size of loess soils is silt, comprising 50–70% by weight, with a sand-to-clay ratio that is lower in weight.

Approximately 12% of the Earth's surface is covered by loess soils. The formation processes, index and engineering properties of these soils vary [1,16]. Figure 1 shows the global distribution of loess soils and indicates the areas in which loess of different geotechnical properties is commonly found. The areas indicated as Region 1 in Figure 1 include the Mississippi and Missouri Basins of North America and the glacial loess of the Carpathian Mountains in Eastern Europe. Region 2 comprises loess deposits originating from the foothills of the Alps in Central Europe and the high-altitude mountains of southern Russia. Region 3 consists of silt grains deposited by winds from deserts in Northern China and the Central Asian Republics [15, 17-19]. In particular, the origin of the desert loess in Region 3 is based on the grains transported by rivers from the surrounding mountains [20-22].

The mineral structure and natural water content play a significant role in the behaviour of loess soils. These soils, defined by a high void ratio and semi-unstable structure at low water content, exhibit high strength in their dry state. The weak clay and calcite bonds that hold loose soil particles together weaken or disappear completely when the soil becomes saturated, causing it to collapse suddenly (hydrocollapse) [23-26]. Oedometer tests were conducted by Nouaouria et al. [3] on loess soils in Algeria, which reported that hydrocollapse increases up to a specific level depending on the applied stress, reaching a maximum at 20-21% water content. In addition, the engineering properties of loess soils have been the focus of investigation by various researchers, taking into account the mineral structure, formation process and grain size distributions [6, 27-29]. Gibbs and Holland [30] reported that the liquid limit (LL) values of loess soils in the Kansas region of the USA, which exhibit cohesive properties, range from 25% to 60%. The plasticity index (PI) ranges from 5% to 37%. The maximum strength is realised at water contents of less than 10%, and the resistance to settlement is high. Xu et al. [31] investigated the critical state parameters of loess soils in North West China with LL ranging from 20% to 35.6% and PI ranging from 6% to 17.1%. They conducted triaxial compression tests to determine these values. Bandyopadhyay [32] examined the permeability of loess soils in the USA and stated that their vertical permeability was much higher

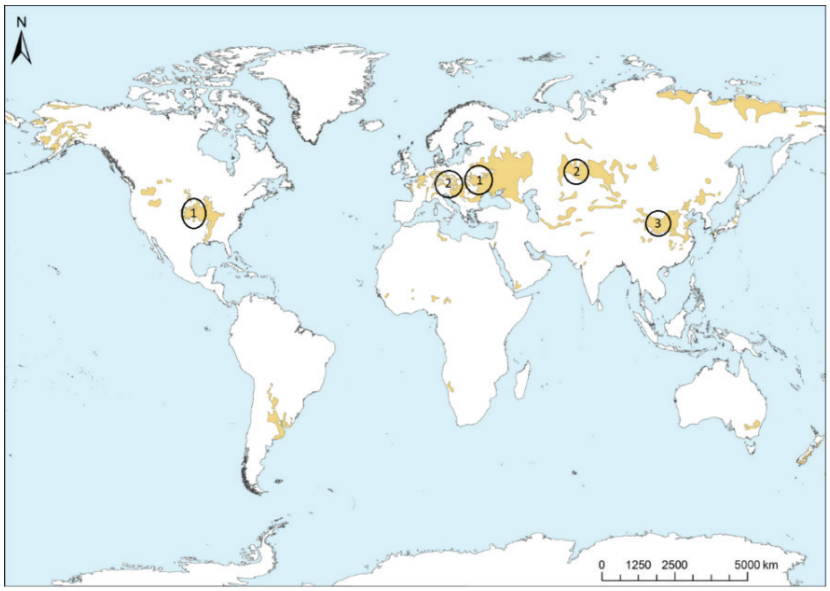

Figure 1. Rich loess soil deposits [22] [created by author].

than their horizontal permeability. However, Terzaghi et al. [9] noted that permeability varies due to changes in the structure of loess soils upon reaching saturation. Chindraprasirt et al. [33] prepared loess soil samples with varying clay contents from Northeast Thailand and subjected them to direct shear box tests. In these tests, where the maximum internal friction angle (ϕ) was found to be 25°, a decrease in the computed ϕ values was observed as the clay content increased. Ma et al. [34] performed CBR tests on 72 loess soil samples prepared with different compaction energies and water contents in China. They reported that samples on the dry side of the optimum density showed higher strength, but soaking the same samples in water resulted in a loss of bearing capacity of up to 97%. Wen and Yan [35] investigated the mechanical properties of unsaturated loess soils in Lanzhou, by conducting direct shear box tests. They highlighted that although significant decreases in measured shear strength and parameters (ϕ, c) were observed due to changes in soil structure, the changes in shear behavior were relatively small. Li et al. [15] carried out a study of the shear strength behaviour of Malan loess soils in China. They reported that the range of cohesion was 0–100 kPa, while the ϕ values varied between 6.5° and 38°. Both parameters were found to decrease with increasing water content and increase with increasing density. Sheeler [36] found that ϕ values varied between 28° and 36° in shear box tests on loess soil samples in the USA. Kong et al. [37] investigated the strength parameters of loess soils with varying grain diameter distributions in Northwest China using direct shear box tests. They reported that the ϕ values varied between 22.2° and 41.5° and that the cohesion changed between 8.3 kPa and 62.2 kPa under differing water contents and vertical stresses.

The analysis of rich loess soil deposits shown in Figure 1 highlights their widespread occurrence in densely populated areas. It emphasises the importance of the index and engineering properties of loess soils for the safe and effective design of structures in these regions. While the relationships between the index and engineering properties of cohesive and granular soils have been demonstrated in numerous studies, the applicability of these findings to silt and loess-type soils remains unclear. Although previous research has explored the characteristics of loess soils, few studies have systematically combined field and laboratory data. In particular, reliable empirical relationships that can be used to estimate the internal friction angle of loess soils from field test results are not widely accepted. To address this gap in the literature, this study investigated the empirical correlations between the internal friction angles obtained from direct shear tests on loess soils collected from Central Asia and Standard Penetration Test (SPT) blow counts. This will enable preliminary estimations in geotechnical design where laboratory testing is limited or unavailable [40-43].

FIELD AND LABORATORY STUDIES

General Site Characteristics and Properties of Loess Soils

The geological structure of the study area has been determined by drilling at pre-determined locations within the site. The findings show that the soils are primarily horizontally stratified, indicating a relatively consistent depositional pattern. Although the stratigraphic profile consists of three distinct soil layers, variations in thickness and composition are observed locally due to topographical and geological factors. Composed of sandy gravel, the upper layer extends to a depth of 3 m. Beneath this layer, between 3m and 6m, is a layer of clayey sand. The thickest layer consists of loess layers located at depths ranging from 3 to 30 metres, containing varying proportions of clay and sand. The variable clay and sand content of these layers has a significant effect on the soil's mechanical properties. In particular, an increase in clay content increases cohesion while reducing ϕ.

The sub-layer at depths between 30 and 36 metres consists of low-plasticity clays containing a certain proportion of loess, with LL% values ranging from 24 to 35%. It is important to emphasise that although this stratigraphic model provides a general framework, the depth and composition of the soil layers may vary locally depending on the geomorphological structure of the site and the depositional history. Detailed in-situ and laboratory investigations, including grain size distribution, Atterberg limits and direct shear box tests, would further improve the understanding of the geotechnical behaviour of these deposits.

Once the density values for the samples obtained from 20 boreholes at different depths had been determined, the samples extracted from the drill tubes were subjected to shear box tests. In consideration of the number of boreholes and their depths, the average depth of the samples tested was determined to be 16.0 m. Following the completion of the shear box tests, the samples were dried at 105°C for a period of 24 hours. The soil samples were then subjected to wet analysis tests. The samples that passed through the No. 200 (0.075 mm) sieve were analysed using a hydrometer, while those that were retained on the No. 200 sieve proceeded to sieve analysis. Consequently, only samples passing through the No. 40 (0.425 mm) sieve at a rate of at least 65% were considered in this study. Therefore, only 86 of the 135 shear box test samples met this criterion and were included in the analysis. The grain size distributions of the soil samples are illustrated in Figure 2.

Table 1 summarizes the specific gravity (Gs), water content (w), grain size percentages, liquid limit (LL), plastic limit (PL), and density (ρ) for 86 soil samples collected at depths ranging from 1.50 m to 36 m, based on ASTM D854-14, ASTM D6938-17, ASTM D6913/D6913M-17 and ASTM D7928-17, ASTM D4318-17, and ASTM D7263-21, respectively. The mean grain size (D_{50}) was determined for each sample, based on the obtained grain diameter distributions [44-49].

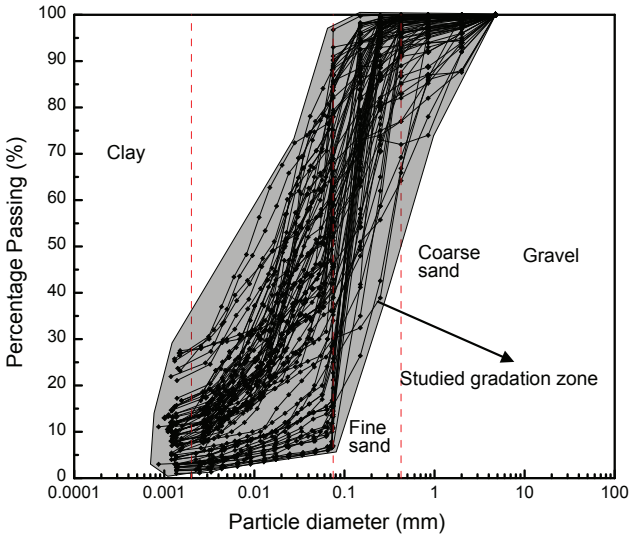

Figure 2. Grain size distribution curves of soils.

Sample Preparation and Direct Shear Test Setup

Soil internal friction angles are generally determined by direct shear box tests or triaxial compression tests, each of which has its own advantages and limitations. Although direct shear testing is less effective than triaxial testing at replicating true in-situ stress paths, it was preferred in this study due to methodological and practical considerations. A total of 405 direct shear tests were conducted on 135 loess samples at different normal stress levels, not including additional repeatability tests. Direct shear testing is faster and easier to handle. It allows samples to be tested at their in-situ water content and density. In contrast, triaxial tests involve highly time-consuming saturation and consolidation stages. Considering the large number of samples tested, direct shear testing was more suitable for achieving the empirical correlation objectives of this study. In this study, the SPT N and ϕ values required to investigate their correlations were determined by following the field and laboratory test procedures outlined below.

1) The SPT blow counts in the study area were determined using an MD300 auger-type water drilling machine equipped with an automatic hammer ram. The values were obtained from a total of different 20 boreholes, each with a diameter of 75 mm, and drilling depths ranging from 13.50 m to 36 m. SPTs were carried out by repeatedly dropping a 63.5 kg hammer from a height of 76.2 cm onto a standard sampler positioned at the upper level of the specified locations. A total of 45 cm of the sampler was allowed to penetrate the soil in three stages. The number of blows required for each 15 cm of penetration was recorded. The first 15 cm was excluded from the analysis as this was considered to be the stage at which the sampler settled in the soil. The total number of blows (N_{30}) was determined by summing the number of blows from the second and third 15 cm penetrations. For these boreholes, the energy rate was considered to be 60%, and the SPT guide rod length was set at 1 m. Following the drilling process, the drill tubes were extracted from the boreholes and sealed with paraffin to preserve the natural water content. The samples were then transferred to the laboratory for the next stage.
2) The density of the soil in the tubes was calculated by weighing the drill tubes, for which both the weight and volume were known. Subsequently, in order to test the homogeneity of the soil in the tubes, the tubes were cut with specialised cutting instruments, and density values were verified by taking samples with thin-walled steel samplers. In the laboratory, the water content of loess soils was found to range from 3.10% to 25.3%. In addition, wet analysis and hydrometer tests revealed that the clay content varied between 5% and 20%. The interplay between these two parameters and capillary effects was found to facilitate the sampling process (Fig. 3. Cylindrical samples were extracted from the drill tube for the sole purpose of calculating their density. It is important to note that these samples were not used in the shear box tests. The evaluation of the processes of taking samples from boreholes under field conditions, transporting them to the laboratory, and sampling in the laboratory environment revealed that the samples had been disturbed. It was therefore decided that the samples be reconstructed to match the water content and density values observed in the field. For this purpose, the soil samples from the tubes were removed and the water content was determined.

Table 1. Summary of the material properties of the soils within the scope of this study

	Gs	w (%)	Depth (m)	ρ (gr/cm³)	LL (%)	PL (%)	Coarse sand (%)	Fine sand (%)	Silt (%)	Clay (%)	D_{50} (mm)
Soil count	86	86	86	86	19	19	86	86	86	86	86
Max.	2.76	25.30	36.0	2.15	35.00	19.30	35.00	93.00	84.20	27.70	0.32
Min.	2.52	3.10	1.50	1.75	24.30	15.20	0.00	3.20	6.00	1.00	0.009
Mean	2.65	15.60	16.00	1.93	28.20	16.71	5.80	39.80	43.90	10.50	0.079

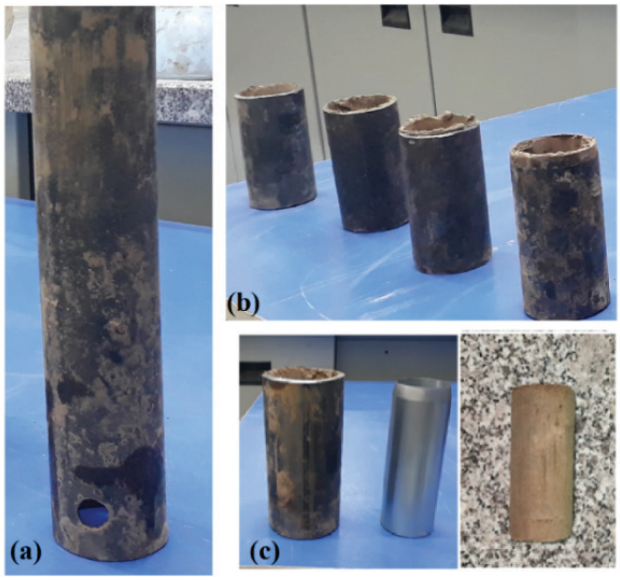

Figure 3. Determination of density a) sample in drill tube b) cutting the drill tube for sampling c) obtaining cylindrical samples.

3) Soil samples with known natural density (ρ) were compacted in a 6 cm x 6 cm x 5 cm shear box ring at a height of 4 cm. For a V=144 cm^3, the amount of soil (M) required for each sample was determined by ρ=M/V. Following the careful placement of all the soil in the ring, the compaction process was initiated. While it is not possible to preserve the microstructure of loess completely after sampling, the reconstituted samples were prepared using field-measured natural density and moisture contents to closely replicate the void ratios and conditions in situ. This methodological approach enables reliable assessment of macroscale geotechnical behaviour, particularly with regard to shear strength parameters. Similar procedures have been adopted in previous loess studies where undisturbed sampling is technically impractical and where controlled reconstitution is widely accepted as a valid alternative for maintaining representation [5, 12]. The reconstituted samples were assumed to represent in situ field conditions; however, no additional validation tests were conducted to quantitatively evaluate the accuracy of this assumption. A rigid plate was positioned to ensure that the loads applied during these compaction processes were distributed homogeneously across the upper level of the soil. As a result of the gradual application of loads to the loading head, the height of the soil in the ring continued until it reached a height of 4 cm. Details of the used for the shear box tests are presented in Figure 4. Displacement and force transducers were used to monitor and record shear strain and force during the test. Normal stress was applied to the top of the lid using a mechanism with a lever ratio of 1:9. The vertical displacement was allowed to complete after the application of the vertical load and then the shear phase started. The upper half of the shear box was fixed while the lower half was forced to move horizontally at a constant rate of 1 mm/min for 10% displacement. To minimize the frictional resistance caused by contact between the upper and lower sections during the shearing process, a 0.05 mm gap was left between the two halves of the direct shear box. In the direct shear test apparatus, adjustment screws are used to create a small gap and minimise friction between the lower and upper boxes. This procedure ensures the formation of a clear shear plane, enhancing reliability by making the measured shear strength parameters independent of box friction.

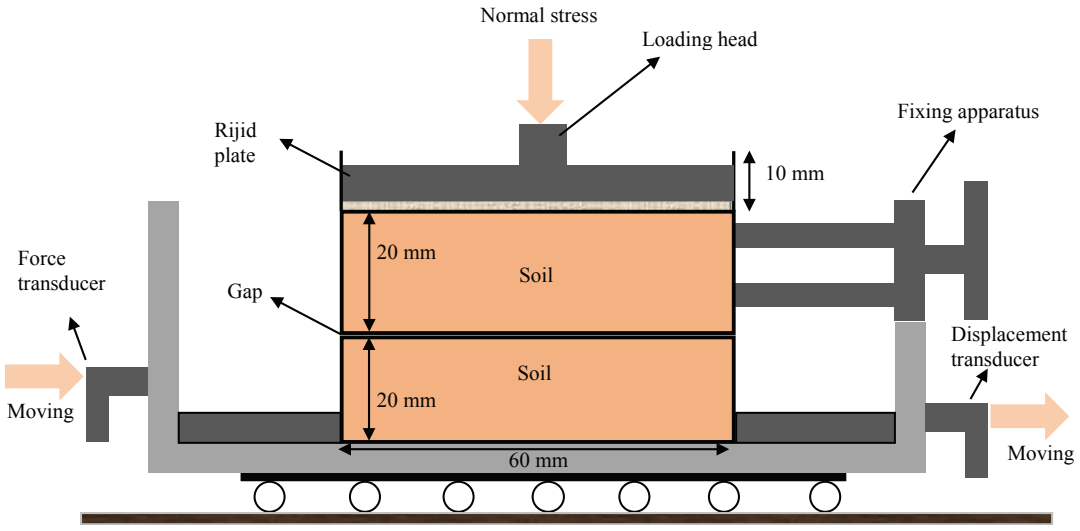

Figure 4. Direct shear test device.

4) The test samples were prepared by compacting and reconstituting them in a direct shear box to reflect the in situ density and moisture content values. The samples were then tested at a cutting speed of 1 mm/min under vertical stresses of 100 kPa, 200 kPa and 400 kPa up to a horizontal strain of 10%. The shearing process was initiated one minute after the application of the vertical normal stresses. Control tests were conducted to assess the repeatability of the results, and the findings were found to be consistent under repeated testing under similar conditions. The final tests were conducted to determine the shear strength parameters, based on 258 direct shear tests performed on 86 soil samples in accordance with ASTM D3080 [50].

RESULTS AND DISCUSSION

A review of the literature reveals a number of studies investigating SPT N–ϕ correlations in sandy soils, as summarized in Table 2. In the equations, N refers to the raw SPT blow count measured directly during field tests. N_1 is the corrected value obtained by applying an overburden correction and considering the effective vertical stress conditions in the soil profile. $N_{(60)}$ represents the SPT blow count standardised by applying energy correction and based on the differing energy transfer efficiencies of the field equipment used. $N_{1(60)}$ denotes the corrected SPT blow count obtained by applying overburden and energy corrections, as well as additional corrections based on the characteristics of the testing equipment used. In the first group of literature, no corrections are applied to the N values and the ϕ values are derived directly from these uncorrected values. The second group of literature applies various corrections to the N values, except for the overburden correction. Finally, the third group of literature applies all corrections to the N values. These different methods highlight the variability in data treatment and its potential impact on the accuracy of ϕ value estimates.

To correctly interpret SPT results under field conditions, it is important to understand the properties of the test equipment and the soil conditions. The measured SPT N values require correction for these factors. Incorrect determination of the N values can result in estimates of soil properties and bearing capacity that are both unsafe and unrealistic [64]. The application of the basic corrections given in Eq. 1 to the field to the N blow count gives the $N_{(60)}$.

$$N_{(60)} = \frac{C_R.C_S.C_B.E_R}{60} * N \quad (1)$$

In Eq. 1; E_R hammer efficiency, C_R rod length correction, C_B borehole diameter correction and C_S sampler correction, C_N overburden correction

In homogeneous soils, both vertical and horizontal effective stresses increase with depth, resulting in higher SPT blow counts. To account for this depth-related influence, an overburden correction factor (C_N) is applied and the corrected blow count is expressed as N_1. Considering the Turkish Building Earthquake Regulations [65] and Liao and Whitman's [66] proposed Equation 2, the C_N values were determined. In this equation, σ'_{v_0} represents the effective vertical stress acting on the test sample, which is calculated by multiplying the relevant sampling depth by the density. As the depth increases, the resulting

Table 2. SPT N versus f correlations recommended for sand soils in literature studies

Correlation type	Referance	Count	Proposed of equation	Limit
SPT N-ϕ	Ferdous [51]	8 samples	ϕ=0.28N + 22.72	-
	Kumar et al. [52]	-	ϕ= 0.2857N + 27.12	4<N<50
	Puri et al. [53]	1053 boreholes	ϕ=0.3128N + 26	1<N<52
	Yusof and Zabidi [54]	14 boreholes	ϕ = 0.481N +29.174	
SPT $N_{(60)}$-ϕ	Wolff [55]	-	$\phi' = 27.1 + 0.3N_{60} - 0.00054\,N^2_{60}$	$N_{60} < 60$
	Japan Road Assoc. [56]	-	$\phi=(15N_{(60)})^{0.5}+15 \leq 45$	N > 5
	Mujtaba et al. [38]	60 boreholes	$\phi=0.7N_{60} + 18$	
SPT $N_{1(60)}$-ϕ	Kuhawy and Mayne [57]	-	$\phi= \tan^{-1}\left(\frac{N_{60}}{12.2+20.3\frac{\sigma'_0}{P_a}}\right)^{0.34}$	$N_{60} < 60$; $\sigma'_v/Pa < 3$
	Hatanaka and Uchida [58]	12 samples	$\phi= (20N_{1(60)})^{0.5} +20$	$N_{1(60)} < 40$
	Mayne [59]	-	$\phi= (15.4N_{1(60)})^{0.5} +20$	-
	Chen [60]	48 samples	$\phi=7.1 \log_{10}[N_{1(60)}]_+ 29.8$	-
	Brown and Hettiarachchi [61]	36 samples	$\phi= 0.3818\tan^{-1}\left(\frac{0.25N_{(60)}xP_a}{\sigma'_0}\right)$	-
	Schnaid et al. [62]	-	$\phi=18\,[N_{1(60)}]^{0.234}$	-
	Ching et al. [63]	-	$\phi=9.2 \log_{10}[N_{1(60)}]_+ 27.5$	-

increase in vertical effective stress leads to a reduction in the C_N. Accordingly, the minimum C_N value of 0.52 was obtained at a depth of 33 m, while the maximum value of 1.70 was calculated at a depth of 1.5 m. Table 3 summarises the correction factors applied to the raw SPT N values obtained using an automated hammer system that provides a consistent energy input during testing. Despite this automation, adjustments are still required to account for variations in C_B, C_S, C_R, E_R, and C_N. These factors are crucial for standardising the number of counts and ensuring that the test results can be compared with those reported in the literature. In addition, Table 3 shows both the standard acceptable ranges and the specific correction values used in this study, which were selected based on relevant geotechnical standards and previous literature. These correction coefficients ensure that the characteristics of the experimental equipment and soil conditions are considered. Improving the accuracy of SPT data significantly enhances the reliability of the correlations between SPT N and ϕ.

$$C_N = 9.78 * \left(\frac{1}{\sigma'_{vo}}\right)^{0.5} < 1.70 \quad (2)$$

Terzaghi et al. (1996) proposed two equations that represent the correlations between SPT N and ϕ [9]. The results of the analysis demonstrate that grain size is a critical parameter that has a significant impact on the relationships under consideration. Salari et al. [67] performed SPT and direct shear tests on 50 gravel samples (25 GC and 25 GW). Based on all the data and the grain size distribution of the gravel, they proposed two equations to describe the relationship between the SPT N and ϕ values If the f value for SPT N-f correlations is determined under laboratory conditions, it is important to ensure that the samples have the same properties as they do under field conditions. Hatanaka and Uchida [58] obtained 12 undisturbed samples by freezing them to preserve their field conditions. They then conducted triaxial tests on these samples to determine their f values. In addition to SPT N-ϕ correlations derived from field and laboratory tests, this relationship has also been explored using various machine learning methods and statistical analyses. Kumar et al. [52] employed the random number generation technique to estimate the ϕ based on the SPT blow counts.

The correlation between the relative density (Dr) of cohesionless soils under field conditions and the N blow count has been investigated by various researchers, resulting in the proposal of several equations to express this relationship [68-70]. Furthermore, the density of the soils and the Dr (%) values are directly related. Therefore, an increase in the density of soils with the same properties will enhance soil resistance, resulting in higher SPT N values and strength. However, the relatively weak correlations shown in Figure 5 are mainly due to the variability in grain size distribution among the samples tested. The mechanical behaviour of soils is directly related to their particle size distribution. However, the variability of soil properties and particle size distributions, combined with the large number of variables, makes it difficult to identify clear statistical trends. When the drilling data is considered, it reveals that the upper layers contain loess soils with a high sand content, whereas the deeper layers consist of clayey loess. Soils with homogeneous grain size distributions generally become denser with increasing depth due to elevated geological stresses, resulting in higher SPT N values and internal friction angles [2, 26, 71]. In this study, however, soils with higher proportions of sand were mostly located at shallower depths. These samples exhibited SPT N values generally greater than 40 and internal friction angles exceeding 35°. Although an overall increase in the amount of fine-grained material is evident as depth increases, this trend is not consistent across all 20 boreholes. In other words, the distribution of grain sizes varied significantly with depth. In addition, increasing geological loads with depth led to higher soil density and compaction, while water content also varied considerably with depth. When considering these variables together, strong and consistent correlations could not be established for the SPT-N–ρ and ϕ–ρ relationships (Fig. 5).

Statistical summary of the SPT N and ϕ values obtained from direct shear box tests of 86 samples is shown in Table 4. The descriptive statistics such as mean ($\bar{x}$), minimum and maximum values (min–max), standard deviation (SD), number of samples (N), skewness coefficient (S) and kurtosis (K) were calculated to evaluate the samples. These parameters provide a solid foundation for assessing the scientific reliability of the correlation analysis and for gaining a comprehensive understanding of the dataset's distribution characteristics.

As seen in Table 4, the SPT N and ϕ values of the 86 samples exhibit a broad distribution range, with a mean SPT N value of 33.7 and a standard deviation of 12.47. In

Table 3. The correction values and the standard ranges

	Correction of the coefficients				
	C_B	**C_S**	**C_R**	**E_R**	**C_N**
Standard range	1.0-1.15	1.0	0.75-1.0	0.70	0-1.70
This study	1.0	1.0	0.75-1.0	0.70	0.52-1.70

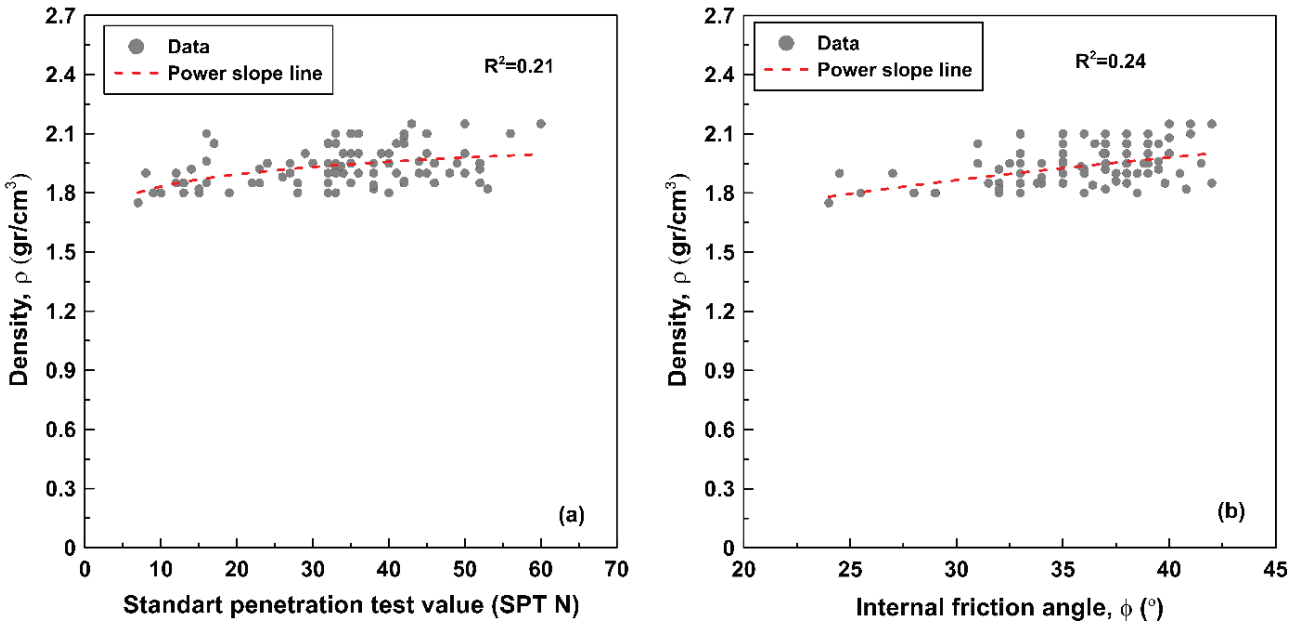

Figure 5. Effect of density on SPT N and ϕ a) SPT N-ρ b) ϕ vs. ρ.

Table 4. Summary of the statistical information from the field and laboratory data

Parameter	Samples (N)	Mean ($\bar{x}$)	Standard deviation (SD)	Minimum (Min.)	Maxiumum (Max.)	Skewness (S)	Kurtosis (K)
SPT N	86	33.71	12.47	7.00	60.0	-0.37	-0.54
SPT N_1	86	28.13	9.85	7.40	54.40	0.35	0.03
SPT $N_{(60)}$	86	37.55	15.38	6.13	68.00	-0.26	-0.76
SPT $N_{1(60)}$	86	30.74	10.79	6.47	58.61	0.18	-0.06
ϕ (°)	86	35.85	3.91	24.00	42.00	-0.95	0.85

contrast, the corrected values SPT N_1 and SPT $N_{1(60)}$ have respective means of 28.13 and 30.74. These results suggest that correction methods have a significant impact on the values. The average internal friction angle is 35.85°, and its skewness (-0.95) and kurtosis (0.85) suggest a left-skewed, peaked distribution. Overall, the limited skewness and kurtosis values suggest that the dataset is suitable for statistical analysis and meaningful interpretation of correlations.

Researchers have used SPT N values to estimate the relative density (Dr) or density of soils [38, 70]. Although this study does not focus directly on density estimation, Figure 6 presents soil density classifications based on the ranges proposed by Terzaghi & Peck [72]. Most of the 86 analysed samples fall within or just above the transition zone between medium-dense and dense soils, indicating that the soils generally have internal friction angles greater than 30°. Samples obtained from shallow depths and composed of coarser grains tend to exhibit higher ϕ values and are positioned near the upper boundary of this classification. However, samples taken from deeper layers with a higher clay content generally exhibit lower ϕ values and are located closer to the lower boundary of the dense soil category.

When field and laboratory test data a evaluated together, it becomes clear that increasing depth results in greater geological loading for samples with similar grain size distributions. This trend has also been observed in direct shear box tests. The samples, which have density ranging from 1.75 to 2.15 g/cm³ and similar grain size distributions, exhibit higher internal friction angles as the density increases. Furthermore, higher SPT N and ϕ values were obtained in samples with a higher sand content when samples were obtained from different depths and possessed similar grain size distributions. The SPT N values were only marginally affected by changes in moisture content. However, direct shear tests showed that an increase in water content, especially in higher

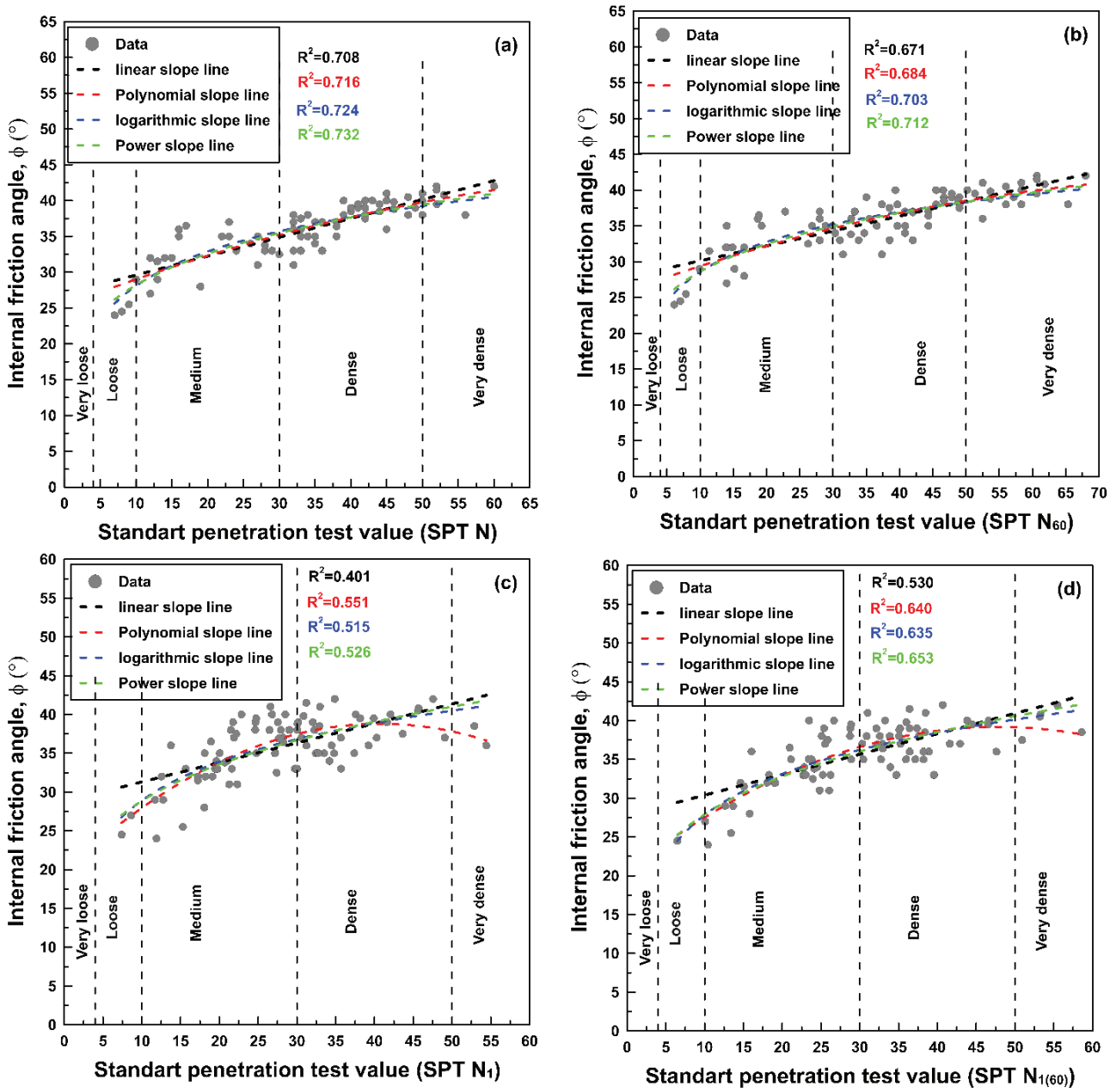

Figure 6. Correlation of SPT N-ϕ a) SPT N-ϕ b) SPT $N_{(60)}$-ϕ c) SPT N_1-ϕ d) SPT $N_{1(60)}$-ϕ.

clay content, reduced the ϕ and led to the development of cohesion. Considering all these findings together, it is clear that there is generally a positive and significant correlation between SPT N and ϕ values. This trend varies depending on the depth of the sample. Samples obtained from depths between 30 and 36 m with a high clay content generally exhibited internal friction angles below 20° and cohesion values of up to 60 kPa. In contrast, samples taken from shallow depths of between 0 and 6 m containing coarser grains showed higher internal friction angles of between 43° and 49°. For this reason, these samples were excluded from the correlation analysis, as their elevated clay or sand content means they do not reflect the typical characteristics of loess.

Table 5 indicates that a variety of regression curves, including linear, polynomial, exponential, and logarithmic, have been used by different researchers. In particular, when examining Figure 6, it is clear that some data points were outliers from the general trend. However, in order not to reduce the number of data points, these outliers were included in the analysis and not excluded. This caused the R^2 to remain at a maximum value of 0.732.

Table 5. SPT N versus f correlations recommended for sand soils in literature studies

Correlation type	Equation type	Equation	Equation ID	R^2
SPT N-ϕ	linear	$\phi=0.264N+26.97$	1a	0.708
	Polynomial	$\phi=-0.002N^2+0.39N+25.33$	1b	0.716
	Logarithmic	$\phi=6.93\ln(N)+12.13$	1c	0.724
	Power	$\phi=17.45N^{0.208}$	1d	0.732
SPT $N_{(60)}$-ϕ	linear	$\phi=0.208N_{(60)}+28.04$	2a	0.671
	Polynomial	$\phi=-0.0018N_{60}^2+0.34N_{(60)}+26.20$	2b	0.685
	Logarithmic	$\phi=6.05\ln(N_{(60)})+14.63$	2c	0.704
	Power	$\phi=18.81\ N_{(60)}^{0.182}$	2d	0.712
SPT N_1-ϕ	linear	$\phi=0.251N_1+28.79$	3a	0.401
	Polynomial	$\phi=-0.0115N_1^2+0.935\ N_1+19.74$	3b	0.550
	Logarithmic	$\phi=7.20\ln(N_1)+12.33$	3c	0.512
	Power	$\phi=17.44\ N_1^{0.218}$	3d	0.526
SPT $N_{1(60)}$-ϕ	linear	$\phi=0.263N_{1(60)}+27.76$	4a	0.530
	Polynomial	$\phi=-0.0082N_{160}^2+0.782N_{1(60)}+20.50$	4b	0.640
	Logarithmic	$\phi=7.65\ln(N_{1(60)})+10.20$	4c	0.635
	Power	$\phi=16.36\ N_{1(60)}^{0.232}$	4d	0.653

When evaluating the performance of the regression curves, it was observed that variations in grain size distribution, water content, and corrections applied to the SPT N values led to significant deviations from the general trend in some samples. However, all data were included in the analyses to improve the representativeness of the natural soil structure observed in the field. In particular, a 70% energy correction was applied for the automatic SPT testing machine used in field conditions for each sample shown in Figure 6b. As the fixed E_R correction affected the N values of all samples by the same proportion, similar R^2 values were obtained for the regression curves in Figures 6a and 6b. In contrast, the C_N correction factor varies between 0.52 and 1.70. For samples where C_N is greater than 1, N values increased, while for samples where C_N is less than 1, N values decreased. This effect increased the scatter of the data in Figures 6c and 6d and significantly reduced the R^2 values. In the analysis findings, the linear regression model showed the lowest correlation, whereas the power regression model generally provided the best fit. These results clearly demonstrate the effect of the correction factors applied to the N values on the selection and performance of the regression models.

The relationship between SPT N-ϕ was investigated in this study, with the results represented by four regression curves, and the corresponding formulations detailed in Table 5. The SPT N blow counts obtained under field conditions were then substituted into these equations to calculate the ϕ values for each sample. In Figure 7, the x-axis represents the ϕ values computed using the equations with the highest R^2 values from Table 5, while the y-axis represents the ϕ values obtained from the shear box tests. Since the R^2 values obtained from Figure 6 are similar (except for Fig. 6c), the variations shown in Figure 7 are closely matched.

The equations proposed by Ferdous [51], Kumar et al. [52], Puri et al. [53], and Yusof and Zabidi [54] for the SPT N-f relationship are applied to loess soils in this study. A comparison of the regression curves derived from these equations with the regression curve based on Equation 1d is shown in Figure 8. A detailed analysis indicates that the regression curve obtained for the soils in this study is aligned closely with the equation proposed by Yusof and Zahidi [54]. While the equation proposed by Kumar et al. [52] and Puri et al. [53] provides compatible results for SPT blow counts between 15 and 50. The equation proposed by Ferdous [51] demonstrates the least compatibility of the three.

The researchers analysing the SPT N-ϕ relationship prefer to utilise different approaches. The application of the SPT $N_{(60)}$-f equations proposed by the researchers to the loess soils considered in this study is presented in Figure 9. The regression curves reveal that the equations proposed by Wolff [55] and the Japan Road Association [56] are compatible with the regression curve developed for the soils in this study within the range of $15 < N_{60} < 50$. In contrast, the equation proposed by Mujtaba et al. [38] displayed the least compatibility.

Table 2 summarises the equations proposed by the researchers, considering the overburden and energy

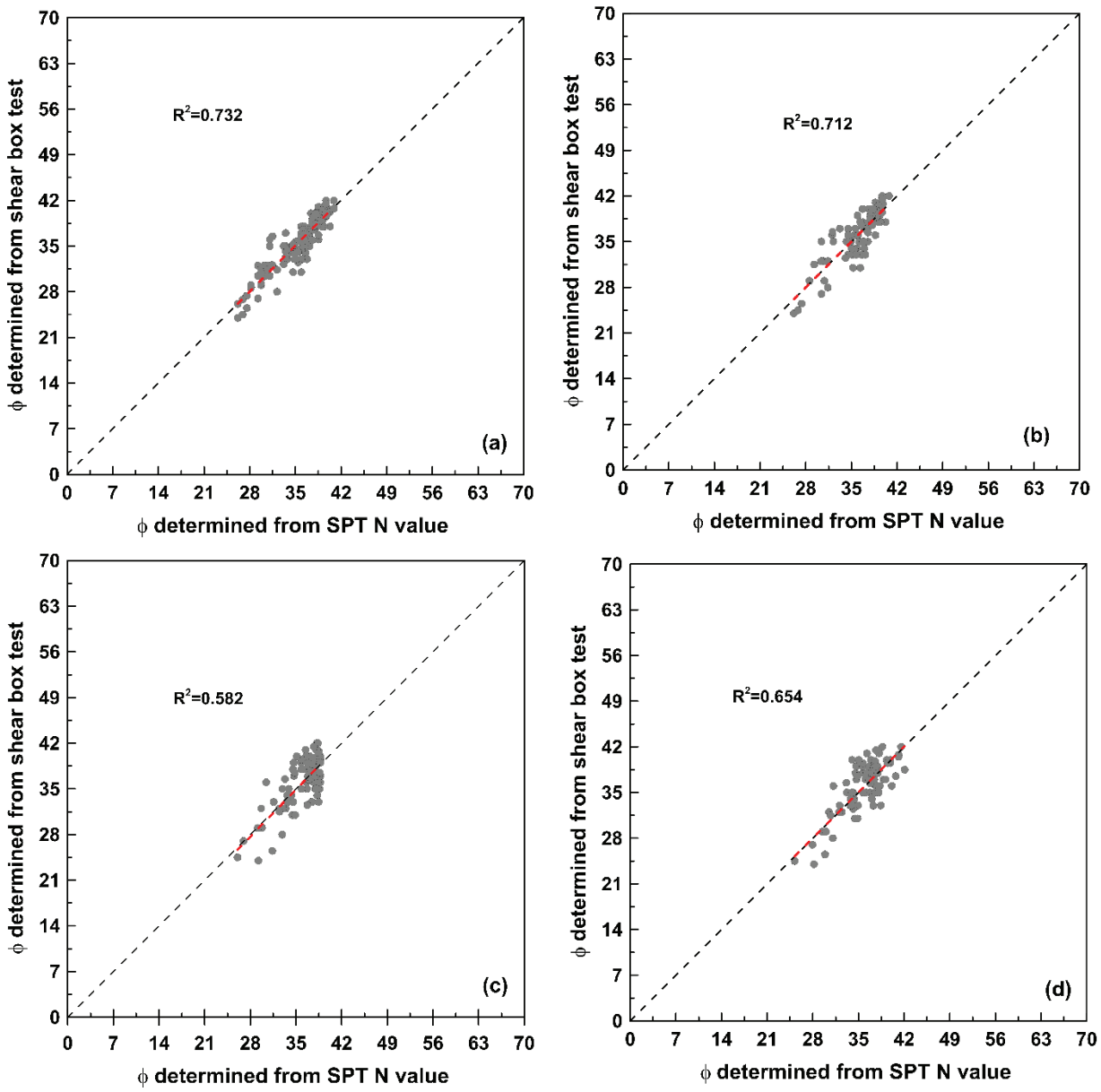

Figure 7. Comparison of ϕ values a) ϕ_{test}- $\phi_{SPT\text{-}N}$ b) ϕ_{test}- $\phi_{SPT\text{-}N(60)}$ c) ϕ_{test}- $\phi_{SPT\text{-}N1}$ d) ϕ_{test}- $\phi_{SPT\text{-}}N_{1(60)}$.

corrections in the field SPT N blow count. The regression curves derived from these equations are shown in Figure 10.

When the curves are analysed, the equations proposed by Kulhawy and Mayne [57], Hatanaka and Uchida [58], Mayne [59], and Chen [60] provide significantly higher f values, while the equation proposed by Brown and Hettiarachchi [61] provides the lowest f values. As a result, none of the equations proposed in the literature for the SPT $N_{1(60)}$-f relationship gave significant results for loess soils. Among these, the equation proposed by Brown and Hettiarachchi [61] seems to be appropriate for loess soils when safety is a priority.

A final discussion of Figures 8-10 indicates that while some of the equations proposed in the literature occasionally provide meaningful results for loess soils, their general applicability is limited. In particular, equations developed on the basis of sandy soils clearly produce inconsistent and unreliable results when applied to loess conditions. This is primarily due to the significant differences in the physical and engineering properties of loess compared to sand. These differences affect the ability of existing empirical equations to accurately describe the behaviour of loess soils, highlighting the need to develop correlations specifically tailored to this soil type.

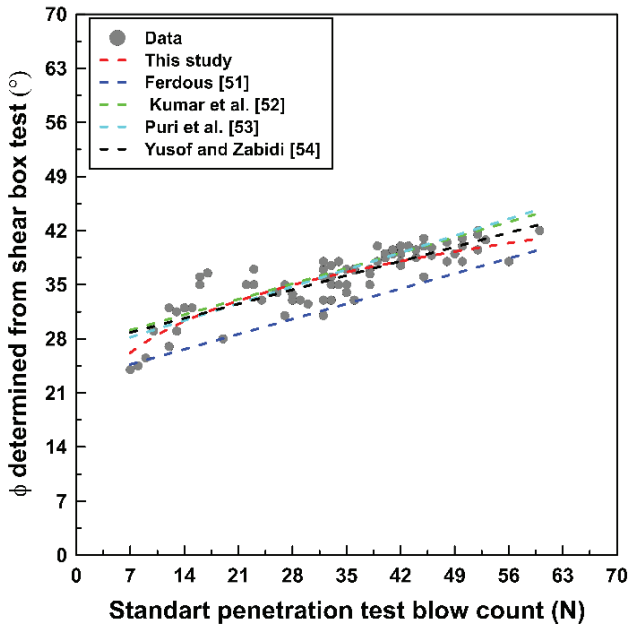

Figure 8. A comparison of regression curves for SPT N-ϕ relationship.

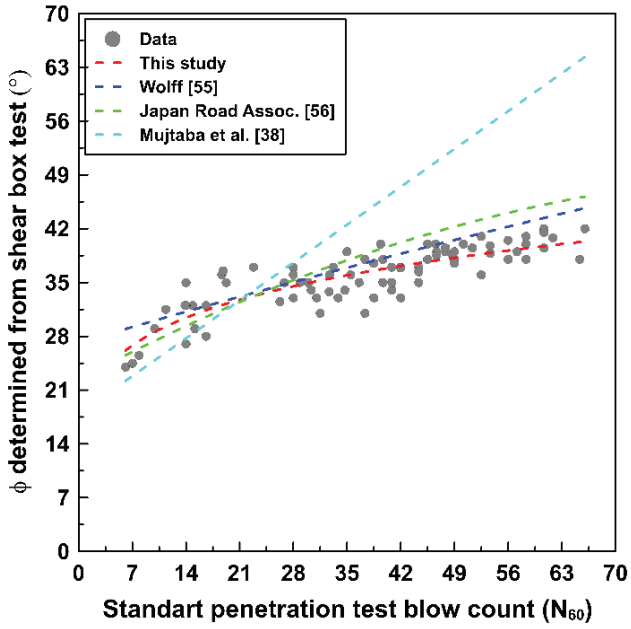

Figure 9. A comparison of regression curves for SPT $N_{(60)}$-ϕ relationship.

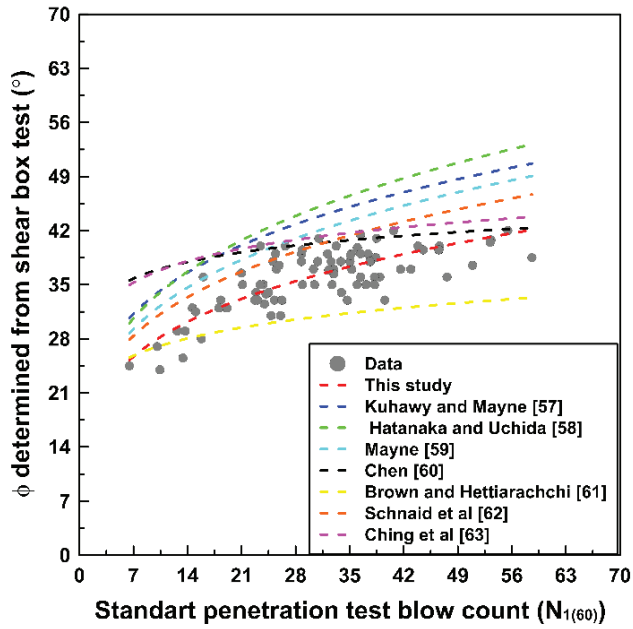

Figure 10. A comparison of regression curves for SPT $N_{1(60)}$-ϕ relationship.

CONCLUSION

The index and strength properties of loess soils are determined through a combination of laboratory and field tests. Although there are sufficient studies that focus on determining the engineering properties of cohesive and granular soils using field tests, research on loess soils remains limited. This study aims to contribute to this topic by determining the internal friction angles from standard penetration test blow counts values obtained in the field for loess soils in Central Asia. The results obtained are summarised below.

1) In consideration of the formation processes of the Central Asian loess, there is a notable variation in grain size distribution. While the majority of grain sizes fall within the range of 0.425 mm to 0.002 mm, there are instances where soils with grain sizes between 4.75 mm and 0.425 mm have been observed at specific depths.
2) Considering the standard penetration test blow counts, these values increased with depth for loess soils with similar grain size distributions. In addition, for loess soils at the same depth in different boreholes, higher standard penetration test blow counts were obtained for samples with larger D_{50} values.
3) Direct shear tests were carried out on samples that were reconstituted to reflect the density and water content of the in situ conditions. The results showed that the ϕ values increased as the density and D_{50} values increased.
4) The SPT-N-ϕ relationship for the loess soil properties considered in this study was examined for different regression models. The determination coefficients representing the different models range from 0.65 to 0.73. These values indicate that ϕ can be estimated from standard penetration test blow counts. Existing SPT N-ϕ correlations, originally established for clean sands, were evaluated for their applicability to loess soils. Although a limited number of studies have achieved satisfactory results, the findings indicate that improved correlations

based on loess soil properties are necessary to enhance the reliability of predictions.

5) These findings provide geotechnical engineers and applicators with practical empirical equations for estimating the internal friction angles of loess soils based on SPT N-values determined under field conditions. The equations contribute to a better understanding of loess soil behaviour in geotechnical site characterisation, foundation design and soil improvement applications during the preliminary design stages or in projects where laboratory testing is limited.

The internal friction angles of loess soils were determined in this study in a laboratory under conditions that reflect in situ density and water content. Meaningful correlations were obtained with standard penetration test blow counts. However, the degree of soil compaction is a critical factor influencing shear strength. Therefore, future studies should include tests representing different levels of compaction to improve the reliability of the correlations and provide a more comprehensive understanding of the engineering behaviour of loess soils.

This study is limited to loess soils in Central Asia. Therefore, the empirical correlations proposed herein are context-specific and unique to the soils studied in this region. They may not be directly applicable to loess soils from regions with different geological origins, mineral compositions, grain size distributions or post-depositional alterations. Therefore, caution should be used when applying these correlations outside the studied context, and validation at the site in question is strongly encouraged.

ACKNOWLEDGEMENT

The author would like to thank M.Sc. Ahmet Serdar Köşeli, M.Sc. Nazlı Ece Öz, Prof. Dr. Havvanur Kılıç, and the staff of the Geotechnical Laboratory at Yıldız Technical University for their contributions to this study.

DATA AVAILABILITY STATEMENT

The authors confirm that the data that supports the findings of this study are available within the article. Raw data that support the finding of this study are available from the corresponding author, upon reasonable request.

CONFLICT OF INTEREST

The author declared no potential conflicts of interest with respect to the research, authorship, and/or publication of this article.

ETHICS

There are no ethical issues with the publication of this manuscript.

STATEMENT ON THE USE OF ARTIFICIAL INTELLIGENCE

Artificial intelligence was not used in the preparation of the article.

REFERENCES

[1] Xie WL, Li P, Zhang MS, Cheng TE, Wang Y. Collapse behavior and microstructural evolution of loess soils from the Loess Plateau of China. J Mt Sci 2018;15:1642–1657. [CrossRef]

[2] Liu Z, Ma X, Zhou D, Lu L, Zhang H, Bai Y, et al. The geological origins and soil properties of loess-like silty clay: A case study in the Jinan area. Sci Rep 2024;14:12612. [CrossRef]

[3] Nouaouria MS, Guenfoud M, Lafifi B. Engineering properties of loess in Algeria. Eng Geol 2008;99:85–90. [CrossRef]

[4] Sharifi Teshnizi E, O'Kelly BC, Karimiazar J, Moosazadeh S, Arjmandzadeh R, Pani A, et al. Effects of cement kiln dust on physicochemical and geomechanical properties of loess soil, Semnan Province, Iran. Arab J Geosci 2022;15:1482. [CrossRef]

[5] Assadi-Langroudi A, Ng'ambi S, Smalley I. Loess as a collapsible soil: Some basic particle packing aspects. Quat Int 2018;469:20–29. [CrossRef]

[6] Hou Y, Li P, Wang J. Review of chemical stabilizing agents for improving the physical and mechanical properties of loess. Bull Eng Geol Environ 2021;80:9201–9215. [CrossRef]

[7] Lian B, Peng J, Zhan H, Wang X. Mechanical response of root-reinforced loess with various water contents. Soil Tillage Res 2019;193:85–94. [CrossRef]

[8] Yuan-jun J, Alam M, Li-Jun S, Umar M, Sadiq S, Jia LJ, et al. Effect of root orientation on the strength characteristics of loess in drained and undrained triaxial tests. Eng Geol 2022;296:106459. [CrossRef]

[9] Terzaghi K, Peck RB, Mesri G. Soil Mechanics in Engineering Practice. 3rd ed. New York: John Wiley & Sons; 1996.

[10] Liu TS. Loess and the Environment. Beijing: China Ocean Press; 1985.

[11] Swineford A, Frye JC. Petrography of the Peoria loess in Kansas. J Geol 1951;59:306–322. [CrossRef]

[12] Rogers CDF, Dijkstra TA, Smalley IJ. Hydroconsolidation and subsidence of loess: Studies from China, Russia, North America and Europe: In memory of Jan Sajgalik. Eng Geol 1994;37:83–113. [CrossRef]

[13] Nemecz E, Pécsi M, Hartyáni Z, Horváth T. The origin of the silt-size quartz grains and minerals in loess. Quat Int 2000;68-71:199–208. [CrossRef]

[14] Alam M, Jiang YJ, Umar M, Su LJ, Rahman M, Ullah F. Influence of drainage and root biomass on soil mechanical behavior in triaxial tests. Acta Geotech 2022;17:3151–3170. [CrossRef]

[15] Li Y, Zhao J, Li B. Loess and Loess Geohazards in China. 1st ed. CRC Press/Balkema; 2018. [CrossRef]
[16] Ajami M, Heidari A, Khormali F, Gorji M, Ayoubi S. Effects of environmental factors on classification of loess derived soils and clay minerals variations, northern Iran. J Mt Sci 2018;15:976–991. [CrossRef]
[17] Smalley I, Catt JA, Davy R, Thomas MF. Rivers and loess: The significance of long river transportation in the complex event-sequence approach to loess deposit formation. Quat Int 2008;181:88–98.
[18] Stevens T, Carter A, Watson TP, Vermeesch P, Andò S, Bird AF, et al. Genetic linkage between the Yellow River, the Mu Us desert and the Chinese Loess Plateau. Quat Sci Rev 2013;78:355–368. [CrossRef]
[19] Marković SB, Fitzsimmons KE, Sprafke T, Gavrilović D, Smalley IJ, Jović V, et al. The history of Danube loess research. Quat Int 2016;399:86–99. [CrossRef]
[20] Muhs DR. Loess and its geomorphic, stratigraphic, and paleoclimatic significance in the Quaternary. In: Shroder JF, editor. Treatise on Geomorphology. Academic Press; 2013. p. 149–183. [CrossRef]
[21] Smalley I, O'Hara-Dhand K, Kwong J. China: Materials for a loess landscape. Catena 2014;117:100–107. [CrossRef]
[22] Fenn K, Prud'Homme C. Dust deposits: Loess. In: Shroder JF, editor. Treatise on Geomorphology. 2nd ed. Academic Press; 2022. p. 320–365. [CrossRef]
[23] Chen ZY. Practical solutions to problems of collapsible loess in China. In: Proceedings of the 7th International Conference on Expansive Soils; 1992; Dallas. Vol 2, p. 1–12.
[24] Parsons RL, Johnson RM, Brown DA, Dapp S, Brennan JJ. Characterization of loess for deep foundations. DFI J 2009;3:14–24. [CrossRef]
[25] Rouaiguia A, Dahim MA. Hydrocollapse of semi-arid soils. Indian Geotech J 2016;46:25–33. [CrossRef]
[26] Hamdy DB. Origin and characteristics of collapsible soils: State-of-the-art report. Innov Infrastruct Solut 2024;9:401. [CrossRef]
[27] Drewnik M, Skiba M, Szymański W, Żyła M. Mineral composition vs. soil-forming processes in loess soils: A case study from Kraków (Southern Poland). Catena 2014;119:166–173. [CrossRef]
[28] Xu L, Coop MR. Influence of structure on the behaviour of a saturated clayey loess. Can Geotech J 2016;53:1026–1037. [CrossRef]
[29] Sun J, Chen R, Qin X, Lou B, Wang Y, Li W. Experimental study on mechanical properties of fissured loess under true triaxial conditions. Sci Rep 2025;15:9852. [CrossRef]
[30] Gibbs HJ, Holland WY. Petrographic and Engineering Properties of Loess (Engineer Monograph No. 28). U.S. Bureau of Reclamation; 1960.
[31] Xu L, Gao C, Zuo L, Liu K, Li L. The critical states of saturated loess soils. Eng Geol 2022;307:106776. [CrossRef]
[32] Chindraprasirt P, Kampala A, Arngbunta A. Engineering characteristics of Khon Kaen loess as construction material. Lowland Technol Int 2020;22.
[33] Bandyopadhyay SS. Geotechnical evaluation of loessial soils in Kansas. Transp Res Rec 1983;945:29–36.
[34] Ma F, Yang J, Bai X. Water sensitivity and microstructure of compacted loess. Transp Geotech 2017;11:41–56. [CrossRef]
[35] Wen B, Yan Y. Influence of structure on shear characteristics of the unsaturated loess in Lanzhou, China. Eng Geol 2014;168:46–58. [CrossRef]
[36] Sheeler JB. Summarization and comparison of engineering properties of loess in the United States. In: Conference on Loess: Design and Construction. Highway Research Board; 1968. p. 1–9.
[37] Kong D, Wan R, Zhao C, Dai J, Dong T, et al. Effect of conglomeration gradation on loess shear strength with different water content. Sci Prog 2021;104(2):00368504211010581. [CrossRef]
[38] Mujtaba H, Farooq K, Sivakugan N, Das BM. Evaluation of relative density and friction angle based on SPT-N values. KSCE J Civ Eng 2018;22:572–581. [CrossRef]
[39] Ghali M, Chekired M, Karray M. Framework to improve the correlation of SPT-N and geotechnical parameters in sand. Acta Geotech 2020;15:735–759. [CrossRef]
[40] Hegde A, Anand A. Resistivity correlations with SPT-N and shear wave velocity for Patna soil in India. Indian Geotech J 2022;52:161–173. [CrossRef]
[41] Ekmen AB. Evaluation of SPT-N values and internal friction angle correlation using artificial intelligence methods in granular soils. Soil Res 2023;61:495–509. [CrossRef]
[42] Alshkane YM. Correlations between geotechnical design parameters and index properties for low-plasticity clays. Transp Infrastruct Geotech 2024;11:3714–3725. [CrossRef]
[43] Guo F, Gu W. Study on dynamic resilient modulus prediction model of subgrade fine-grained soil based on physical property parameters. Sci Rep 2025;15:17605. [CrossRef]
[44] ASTM International. ASTM D854-14: Standard Test Methods for Specific Gravity of Soil Solids by Water Pycnometer. ASTM International; 2023.
[45] ASTM International. ASTM D6938-17: Standard Test Method for In-Place Density and Water Content of Soil and Soil-Aggregate by Nuclear Methods (Shallow Depth). ASTM International; 2023.
[46] ASTM International. ASTM D6913/D6913M-17: Standard Test Methods for Particle-Size Distribution (Gradation) of Soils Using Sieve Analysis. ASTM International; 2023.
[47] ASTM International. ASTM D7928-17: Standard Test Method for Particle-Size Distribution (Gradation) of Fine-Grained Soils Using the Sedimentation (Hydrometer) Analysis. ASTM International; 2023.

[48] ASTM International. ASTM D4318-17: Standard Test Methods for Liquid Limit, Plastic Limit, and Plasticity Index of Soils. ASTM International; 2023.
[49] ASTM International. ASTM D7263-21: Standard Test Methods for Laboratory Determination of Density (Unit Weight) of Soil Specimens. ASTM International; 2023.
[50] ASTM International. ASTM D3080/D3080M–11: Standard test method for direct shear test of soils under consolidated drained conditions. West Conshohocken, PA: ASTM International; 2011.
[51] Ferdous S. Geotechnical Characterization of the Subsoil in Khulna City Corporation (KCC) Area [MSc thesis]. Bangladesh University; 2007.
[52] Kumar R, Bhargava K, Choudhury D. Estimation of engineering properties of soils from field SPT using random number generation. INAE Lett 2016;1:77–84. [CrossRef]
[53] Puri N, Prasad HD, Jain A. Prediction of geotechnical parameters using machine learning techniques. Procedia Comput Sci 2018;125:509–517. [CrossRef]
[54] Yusof NQAM, Zabidi H. Reliability of using standard penetration test (SPT) in predicting properties of soil. J Phys Conf Ser 2018;1074:012086. [CrossRef]
[55] Wolff TF. Pile capacity prediction using parameter functions. In: Predicted and Observed Axial Behavior of Piles: Results of a Pile Prediction Symposium. ASCE; 1989. p. 96–106.
[56] Japan Road Association. Specifications for Highway Bridges, Part IV. Japan Road Association; 1990.
[57] Kulhawy FH, Mayne PW. Manual on Estimating Soil Properties for Foundation Design. Report No. EPRI-EL-6800. Palo Alto, CA: Electric Power Research Institute; 1990.
[58] Hatanaka M, Uchida A. Empirical correlation between penetration resistance and internal friction angle of sandy soils. Soils Found 1996;36:1–9. [CrossRef]
[59] Mayne PW. Stress-strain-strength-flow parameters from enhanced in-situ tests. In: Proceedings of the International Conference on In-Situ Measurements of Soil Properties and Case Histories; 2001; Bali, Indonesia. p. 27–48.
[60] Chen JR. Axial Behavior of Drilled Shafts in Gravelly Soils [PhD thesis]. Cornell University; 2004.
[61] Brown T, Hettiarachchi H. Estimating shear strength properties of soils using SPT blow counts: An energy balance approach. ASCE Geotech Spec Publ 1998;179:16–26.
[62] Schnaid F, Odebrecht E, Rocha MM, de Paula Bernardes G. Prediction of soil properties from the concepts of energy transfer in dynamic penetration tests. J Geotech Geoenviron Eng 2009;135:1092–1100. [CrossRef]
[63] Ching J, Lin GH, Chen JR, Phoon KK. Transformation models for effective friction angle and relative density calibrated based on generic database of coarse-grained soils. Can Geotech J 2016;54:481–501. [CrossRef]
[64] Sivrikaya O, Toğrol E. Relationships between SPT-N value and undrained shear strength of fine-grained soils in Turkey. Teknik Dergi 2007;18:4229–4246.
[65] Disaster and Emergency Management Authority (AFAD). Turkish Building Earthquake Code (TBEC). Off Gaz Repub Turkey 2018;30364.
[66] Liao S, Whitman RV. Overburden correction factor for SPT in sand. J Geotech Eng 1986;112:373–377. [CrossRef]
[67] Salari P, Lashkaripour G, Ghafoori M. Presentation of empirical equations for estimating internal friction angle of SP and SC soils in Mashhad, Iran using standard penetration and direct shear tests and comparison with previous equations. Int J Geogr Geol 2015;4:89–102. [CrossRef]
[68] Meyerhof GG. Penetration tests and bearing capacity of cohesionless soils. J Geotech Eng Div ASCE 1956;82:866/1–866/19. [CrossRef]
[69] Kibria S, Masood T. SPT, relative density and PHI relationships for Indus sands at Chashma. In: Proceedings of VII National Conference of Pakistan National Society for Soil Mechanics and Foundation Engineering; 1998. p. 169–188.
[70] Cubrinovski M, Ishihara K. Empirical correlation between SPT N-value and relative density for sandy soils. Soils Found 1999;39:61–71. [CrossRef]
[71] Kabir ME, Sabab SR, Bondhon MMM, Shuvo NA. Determining Relations Between SPT-N & Shear Strength Parameters of Dhaka and Sylhet Soils Using Machine Learning Approach [BSc thesis]. Islamic University of Technology; 2022.
[72] Terzaghi K, Peck RB. Soil Mechanics in Engineering Practice. 2nd ed. New York: Wiley; 1967.